

Research Paper

An Endogenous Vaccine Based on Fluorophores and Multivalent Immunoadjuvants Regulates Tumor Micro-Environment for Synergistic Photothermal and Immunotherapy

Ling Li*, Suleixin Yang*, Linjiang Song, Yan Zeng, Tao He, Ning Wang, Chuan Yu, Tao Yin, Li Liu, Xiawei Wei, Qinjie Wu, Yuquan Wei, Li Yang, Changyang Gong[✉]

State Key Laboratory of Biotherapy and Cancer Center, West China Hospital, Sichuan University, and Collaborative Innovation Center for Biotherapy, Chengdu, 610041, P. R. China

*These authors contributed equally to this work.

✉ Corresponding author: E-mail: chyong14@163.com

© Ivyspring International Publisher. This is an open access article distributed under the terms of the Creative Commons Attribution (CC BY-NC) license (<https://creativecommons.org/licenses/by-nc/4.0/>). See <http://ivyspring.com/terms> for full terms and conditions.

Received: 2017.02.26; Accepted: 2017.08.29; Published: 2018.01.01

Abstract

Recently, near-infrared (NIR) light-based photothermal therapy (PTT) has been widely applied in cancer treatment. However, in most cases, the tissue penetration depth of NIR light is not sufficient and thus photothermal therapy is unable to completely eradicate deep, seated tumors inevitably leading to recurrence of the tumor. Due to this significant limitation of NIR, improved therapeutic strategies are urgently needed.

Methods: We developed an endogenous vaccine based on a novel nanoparticle platform for combinatorial photothermal ablation and immunotherapy. The design was based on fluorophore-loaded liposomes (IR-7-lipo) coated with a multivalent immunoadjuvant (HA-CpG). In vitro PTT potency was assessed in cells by LIVE/DEAD and Annexin V-FITC/PI assays. The effect on bone marrow-derived dendritic cells (BMDC) maturation and antigen presentation was evaluated by flow cytometry (FCM) with specific antibodies. After treatment, the immune cell populations in tumor micro-environment and the cytokines in the serum were detected by FCM and Elisa assay, respectively. Finally, the therapeutic outcome was investigated in an animal model.

Results: Upon irradiation with 808 nm laser, IR-7-lipo induced tumor cell necrosis and released tumor-associated antigens, while the multivalent immunoadjuvant improved the expression of co-stimulatory molecules on BMDC and promoted antigen presentation. The combination therapy of PTT and immunotherapy regulated the tumor micro-environment, decreased immunosuppression, and potentiated host antitumor immunity. Most significantly, due to an enhanced antitumor immune response, combined photothermal immunotherapy was effective in eradicating tumors in mice and inhibiting tumor metastasis.

Conclusion: This endogenous vaccination strategy based on synergistic photothermal and immunotherapy may provide a potentially effective approach for treatment of cancers, especially those difficult to be surgically removed.

Key words: photothermal, immunotherapy, vaccine, tumor micro-environment

Introduction

Photothermal therapy (PTT), employing light-absorbing agents to generate heat from near-infrared

(NIR) light energy sources, represents a new approach for cancer therapy [1]. In the past decade, many types

of NIR-responsive materials including inorganic and organic substances, such as carbon nanotubes (CNTs), gold nanoparticles, copper sulfide (CuS), and Indocyanine Green (ICG) and its analogue (IR780, IR808), have been extensively explored for PTT treatment of cancer [2-5]. However, the major challenge in PTT of cancer is the limited penetration depth of NIR light. The effective penetration depth of NIR light is usually limited to no deeper than 1 cm [1]. Therefore, non-irradiated tumor cells in the deep can survive and inevitably lead to tumor recurrence.

PTT of cancer is known to induce tumor cell necrosis and apoptosis. Necrosis of tumor cells releases tumor-associated antigens into the surrounding milieu, a phenomenon called "endogenous vaccination", which can be utilized to trigger specific antitumor immunity for removing the residual tumor residue [6]. The endogenous molecules released after necrosis, known as danger-associated molecular patterns (DAMPs), can trigger the activation of pattern-recognition receptors (PRRs) [7-9]. On the other hand, tumor growth is also associated with immunosuppressive micro-environment, which inhibits tumor antigen recognition, presentation, and the activity of effector cells. The immunosuppression networks include regulatory T (Treg) cells, myeloid derived suppressor cells (MDSC) and type 2 (M2) macrophages, as well as the immunosuppressive cytokines, IL-10 and transforming growth factor- β (TGF- β) [10]. Thus, approaches to specifically modify or normalize the immunosuppressive tumor microenvironment are vital for an effective immunotherapy.

We hypothesized that PTT combined with immunotherapy might be a more effective approach to improve the therapeutic effect of PPT for cancer treatment. In this respect, Wang et al. reported immunological responses triggered by photothermal therapy with carbon nanotubes in combination with anti-CTLA-4 therapy to inhibit cancer metastasis [11]. Guo et al. designed a near-infrared light-induced transformative nanoparticle platform based on chitosan-coated hollow CuS nanoparticles. The results indicated that in a mouse breast cancer model, combined photothermal immunotherapy was more effective than either immunotherapy or photothermal therapy alone [6].

Immunoadjuvants are pharmacological or immunological agents that potentiate the immune responses to an antigen and/or modulate it towards the desired immune responses. Among them, synthetic oligodeoxynucleotides (ODNs) containing the unmethylated cytosine-phosphate-guanine (CpG) motif are an attractive candidate adjuvant for cancer vaccination [12-13]. They bind to Toll-like receptor 9

(TLR9) of antigen presenting cells (APCs), and promote the expression of co-stimulatory molecules as well as the secretion of inflammatory cytokines. Previous reports have indicated that CpG ODNs can directly inhibit the immunosuppressive functions of MDSCs and cause them to differentiate into macrophages with antitumor activity [14-15]. A recent study has also demonstrated that multivalent display of CpG ODNs via grafting these sequences to hyaluronic acid (HA-CpG) can induce much stronger immune-stimulatory activity than CpG ODNs alone through the continuous stimulation of TLR9 [16].

In the present study, we describe an endogenous vaccine based on a novel nanoparticle platform for combinatorial photothermal ablation and immunotherapy. The design is based on fluorophores-loaded liposomes (IR-7-lipo) coated with a multivalent immunoadjuvant (HA-CpG) (Figure 1). IR-7 is an original NIR heptamethine cyanine dye for synchronous cancer PDT and PTT treatment with high phototherapeutic efficacy and few side effects upon 808 nm laser exposure [17]. In a mouse colon cancer model IR-7-lipo/HA-CpG-mediated photothermal immunotherapy induced more effective anti-tumor effects compared with photothermal therapy alone (IR-7-lipo). IR-7-lipo/HA-CpG could significantly reduce the number of MDSCs after NIR irradiation and increase the number of CD8⁺ effector T cells. After a single administration, the combined photothermal immunotherapy was effective in eradicating tumors. There are few reports about combining PTT with immunoadjuvants, which recruit inflammatory-associated cells or promote the maturation of APCs. This strategy based on combination PTT with immunoadjuvants could improve the immune responses in the early stage. Therefore, we believe that this endogenous vaccination strategy based on synergistic photothermal and immunotherapy may provide a potentially effective approach for cancer treatment.

Materials and Methods

Materials and cell lines

1,2-distearoyl-*sn*-glycero-3-phosphocholine (DSPC), 20 α -hydroxycholesterol (Chol), and 1,2-dioleoyl-3-trimethylammonium-propane (DOTAP) were purchased from Avanti Polar Lipids, Inc. *N*-hydroxysuccinimide (NHS), 1-(3-dimethylamino-propyl)-3-ethylcarbodiimide hydrochloride (EDCI) were obtained from Sigma-Aldrich. Sodium hyaluronate (HA) with an average molecular weight of 35 kDa was provided by Shandong Freda Biochem Co., Ltd. (Shandong, China). DNA oligonucleotides were synthesized by Shanghai Sangon Biological

Engineering Technology&Services (Shanghai, China). The sequences were as follows: CpG ODNs 1826-NH₂: 5'-TCCATGACGTTCTGACGTT-NH₂-3'. All other reagents were used as received without further purification. Annexin V-FITC/PI apoptosis detection kit was provided by Nanjing KeyGen Biotech. Co., Ltd (Nanjing, China). LIVE/DEAD® Viability/Cytotoxicity Kit was purchased from Invitrogen (USA). FITC anti-mouse CD40 antibody, PE anti-mouse CD86 antibody, PE anti-mouse H-2K^d antibody, PE anti-mouse I-A/I-E antibody, FITC anti-mouse CD4 antibody, FITC anti-mouse CD8a antibody, FITC anti-mouse/human CD11b antibody, PE anti-mouse CD11c antibody, PE anti-mouse F4/80 antibody, and PE anti-mouse Ly-6G/Ly-6C (Gr-1) antibody were all obtained from BioLegend.

RMPI 1640 medium and fetal bovine serum (FBS) were purchased from GIBCO/BRL Life Technologies. The mouse colon cancer cells CT26 were cultured in RMPI 1640 supplemented with 10%

FBS, 1% penicillin, and 1% streptomycin. Cells were incubated in a humidified incubator at 37 °C with 5% CO₂.

Preparation of IR-7-lipo

IR-7-lipo formulation was prepared using the lipid film hydration method. Briefly, DSPC (4.28 mg), Chol (2.28 mg), DOTAP (0.35 mg) and IR-7 (0.60 mg) were dissolved in chloroform/methanol (v/v = 2:1). The organic solvents were evaporated using a rotary evaporator and the film was dried in a vacuum drier overnight. The resulting thin lipid film was hydrated in 5% glucose solution at 37 °C followed by sonication with a probe sonicator at 80 W for 120 s to form the IR-7-lipo. The IR-7 content in the liposome was determined by UV-Vis spectroscopy. IR-7 loading was defined using the following equation:

$$\text{IR-7 content (\%, w/w)} = \left(\frac{\text{IR-7 weight in IR-7-lipo}}{\text{total IR-7-lipo weight}} \right) \times 100.$$

All measurements were performed in triplicate.

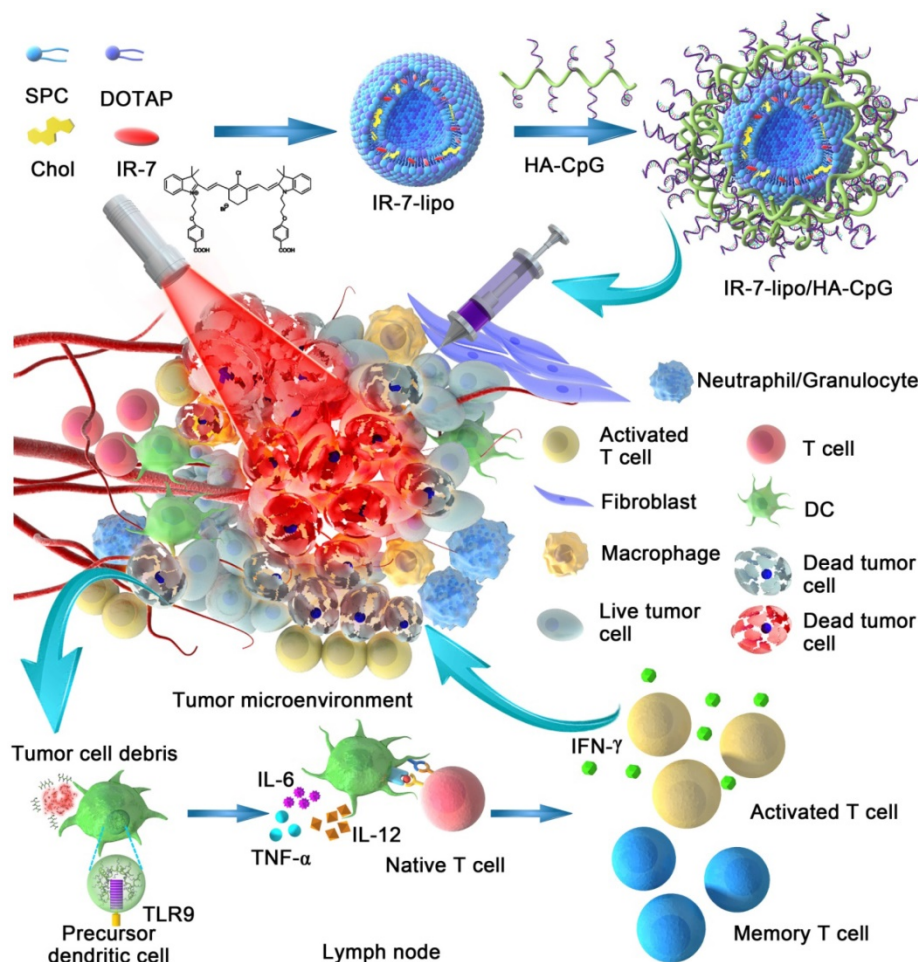


Figure 1. Schematic presentation of synergistic photothermal and immunotherapy by IR-7-lipo/HA-CpG. Local injection of IR-7-lipo/HA-CpG and laser irradiation generate necrosis of tumor cells releasing tumor-associated antigens. The multivalent immunoadjuvant HA-CpG can be recognized by Toll-like receptor 9 (TLR9), trigger multivalent ligand-receptor interaction, promote the maturation and antigen presentation of antigen-presenting cells (APCs), activate the immunosuppressive tumor micro-environment and induce powerful antitumor immune responses removing the tumor residues.

The photothermal conversion efficiency of the IR-7-lipo was measured by a similar method published by Roper et al [18]. The temperature change of IR-7-lipo (25 $\mu\text{g mL}^{-1}$) was recorded as a function of time under continuous 808 nm laser exposure with a power density of 2.0 W cm^{-2} for 5 min. The aqueous dispersion of IR-7-lipo exhibited the steady temperature elevation of 20 °C. Subsequently, 808 nm laser was shut off, and the temperature decrease was monitored to determine the rate of heat transfer from the dispersion system to the environment.

Preparation and characterization of HA-CpG

HA-CpG was synthesized by carbodiimide chemistry at the carboxyl groups of HA and the amino groups of CpG ODNs 1826-NH₂ via amidation reaction. In brief, HA was dissolved in 2-(N-morpholino) ethanesulfonic acid (MES) buffer (0.1 M, pH 6.5). NHS and EDCI were then added to the HA solution and stirred for 2 h to activate the carboxyl groups of HA. Subsequently, CpG ODNs 1826-NH₂ was added to the activated HA. The above mixture was allowed to react at 4 °C for 24 h and dialyzed against distilled water with a dialysis membrane (MWCO, 8000-14000 Da) for 3 days at 4 °C, followed by lyophilization. The product was further characterized by ¹H-NMR and FTIR. The content of CpG ODNs conjugated to HA polymer was quantified with NanoDrop 2000 (Thermo Scientific).

Preparation and characterization of IR-7-lipo/HA-CpG

IR-7-lipo/HA-CpG was prepared by simply mixing IR-7-lipo with HA-CpG via electrostatic interaction. The size and zeta potential of IR-7-lipo and IR-7-lipo/HA-CpG were measured with a dynamic light scattering (DLS) instrument (Malvern Zetasizer Nano-S, Malvern Inc., UK). The morphology of the prepared IR-7-lipo/HA-CpG was further observed using transmission electron microscopy (TEM) (JEOL JEM-100CX, Japan).

In vitro PTT

For LIVE/DEAD assay, CT26 cells were seeded into 6-well plates at the density of 3×10^5 per well. Next, 25 μL of 5% glucose or IR-7-lipo was added to the culture media at the final concentration of 5 $\mu\text{g mL}^{-1}$ of IR-7 and incubated for 3 h. Subsequently, the culture media were removed and the cells were rinsed with PBS three times followed by exposure of one part of the cells in the well to the 808 nm laser irradiation at a power density of 1.0 W cm^{-2} for 5 min. After irradiation, the cells were cultured for another 4 h. The PTT cytotoxicity in CT26 cells was investigated with LIVE/DEAD® Viability/Cytotoxicity Kit.

To analyze necrosis, CT26 cells (1×10^5 cells per well) were seeded into 24-well plates and incubated overnight. Then 6 μL of 5% glucose or IR-7-lipo were added to the culture media at the final concentration of 5 $\mu\text{g mL}^{-1}$ of IR-7 and incubated for 3 h. Subsequently, the culture media were removed and the cells were washed with PBS three times. Following treatment with 5% glucose or IR-7-lipo, few wells were exposed to the 808 nm laser irradiation (1.0 W cm^{-2} , 5 min), while others without laser exposure were used as controls. After irradiation, the cells were further cultured for another 4 h. Subsequently, the cells were trypsinized, washed twice with cold PBS, and resuspended in 500 μL of binding buffer. 5 μL of FITC-conjugated Annexin-V and 5 μL of PI were added. After incubation for 10 min at room temperature, the samples were immediately analyzed by FCM (flow cytometry).

Generation of bone marrow-derived dendritic cells (BMDCs)

BMDCs were isolated from 6-week-old BALB/c mice as previously described with some modifications [20-21]. Mice were euthanized, and the femurs and tibiae were collected. The intact bones were soaked in 75 % (v/v) ethanol for 2 min for disinfection and were then washed with RPMI 1640 medium. Next, both ends of the bones were cut, and the bone marrow was flushed with RPMI 1640 medium using a 1 mL syringe with a 26 G needle. Clusters within the marrow suspension were disintegrated by vigorous pipetting and then passing through a 70- μm nylon cell strainer. The harvested cells were centrifuged at 1500 rpm for 5 min, and the resulting pellet was resuspended in 5 mL of Red Blood Cell Lysis Buffer (Sigma-Aldrich) to deplete erythrocytes. The cells were counted, resuspended, and transferred to Petri dishes containing 10 mL of RPMI 1640 medium supplemented with 20 ng mL^{-1} mouse recombinant granulocyte macrophage colony-stimulating factor (GM-CSF, PeproTech, Rocky Hill, NJ) and 10 ng mL^{-1} IL-4 (PeproTech, Rocky Hill, NJ). Media were replaced every 2 days. On day 6, the aggregates of immature DCs were collected and then DC purity was determined by Flow cytometry (BD Calibur). The percentage of CD11c⁺ cells in these preparations was > 85%.

DC maturation and antigen presentation

For the DC maturation assay, immature BMDCs were pre-plated into 6-well plates at the density of 1×10^6 cells per mL. Then the cells were incubated with IR-7-lipo, HA-CpG, IR-7-lipo/HA-CpG for 24 h at 37 °C. In the IR-7-lipo+laser and IR-7-lipo/HA-CpG+laser treatment group, the cells were

pre-incubated with IR-7-lipo or IR-7-lipo/HA-CpG before laser exposure. Subsequently, the CT26 cancer cells and supernatants after PTT were collected and co-incubated with BMDCs. Cells were harvested and stained with FITC anti-mouse CD40 antibody or PE anti-mouse CD86 antibody for 30 min on ice. Cells were washed with PBS and the expression levels of co-stimulators (CD40, CD86) on the surface of BMDCs were detected on a BD Calibur flow cytometer. For antigen presentation analysis, CT26 cancer cells and supernatants obtained after treatment with different formulations followed by PTT were co-cultured with BMDCs for 24 h at 37 °C. Subsequently, BMDCs were carefully separated and stained with PE anti-mouse H-2K^d antibody or PE anti-mouse I-A/I-E antibody to determine the expression of MHC class I and MHC class II molecules.

Animal model

The female BALB/c mice (6 weeks, 18-22 g) were provided by the Vital Laboratory Animal Center (Beijing, China). The study protocol was approved by the Institutional Animal Care and Use Committee of Sichuan University. CT26 tumor models were established by subcutaneous injection of 1×10^6 CT26 cells on the right flank of BALB/c mice. When the tumor sizes reached about 100 mm³, the mice were randomly divided into five groups (n = 5 per group) for various treatment: 5% glucose + laser (i), IR-7-lipo (ii), IR-7-lipo/HA-CpG (iii), IR-7-lipo + laser (iv), IR-7-lipo/HA-CpG + laser (v). For laser treatment groups, the mice received NIR laser irradiation (808 nm, 2.0 W cm⁻², 5 min) after intratumoral injection. The tumor surface temperatures were monitored by an IR thermal camera (Fluke, USA).

Regulation of tumor micro-environment and cytokine detection

Tumors were harvested at 48 h after intratumoral administration and treated with collagenase I (1 mg/mL, Gibco, USA) for 2 h. Then, the cells were filtered through 70- μ m nylon cell strainers and washed three times with PBS. The single-cell suspension was incubated with FITC anti-mouse CD4 antibody, FITC anti-mouse CD8a antibody, FITC anti-mouse/human CD11b antibody, PE anti-mouse CD11c antibody, PE anti-mouse F4/80 antibody, PE anti-mouse Ly-6G/Ly-6C (Gr-1) antibody for 30 min on ice and then subjected to FCM analysis (BD Calibur). For spleen, the cells were immediately filtered through 70- μ m nylon cell strainer, washed with PBS and stained with FITC anti-mouse CD4 antibody, FITC anti-mouse CD8a antibody. The data analysis was carried out using FlowJo software.

For cytokine detection, serum samples were withdrawn from mice at 24 h, 72 h and 168 h after various treatments. Tumor necrosis factor- α (TNF- α), IL-12 and IL-6 in the serum were analyzed with ELISA kits.

In vivo PTT

The CT26 tumor models were established as mentioned above. The tumor sizes and body weights were measured every 3 days and the tumor volume was calculated according to the equation: Volume = (Tumor Length) \times (Tumor Width)² / 2. At day 15 after treatments, the mice were sacrificed. Tumors and major organs (heart, liver, spleen, lung, and kidney) of mice were harvested for histology analysis.

Statistical Analysis

Data were presented as mean \pm standard deviation (SD). Student's t-test with Bonferroni corrections following ANOVA was applied to analysis for the significance of the difference between two groups. Chi square analysis was used for analyzing percentages. Significant differences between groups were indicated by *p < 0.05, **p < 0.01 and ***p < 0.001, respectively.

Results and Discussion

As shown in Figure 1, IR-7, a hydrophobic chemical was almost insoluble in water. This characteristic largely limited its application *in vivo*. In this study, we prepared liposomes by lipid film hydration and encapsulated IR-7 in these liposomes (IR-7-lipo) to increase its water dispersibility. The content of IR-7 in liposomes was approximately 8% determined by UV/Vis absorption spectra. The average hydrodynamic size of IR-7-lipo was 102.0 ± 12.0 nm by DLS measurement (Figure 2A). The zeta potential of IR-7-lipo was about +34.3 mV, indicating the positively charged DOTAP had been successfully inserted into the liposomes (Figure 2B).

Additionally, to obtain the multivalent immunoadjuvant (HA-CpG), HA was used as the graft polymer to conjugate CpG ODNs. The amino groups of CpG ODNs were conjugated to the carboxyl groups of HA using carbodiimide chemistry (Figure S1, Supporting Information). The successful conjugation was confirmed by ¹H-NMR and FTIR analyses (Figure S2, Supporting Information). Subsequently, HA-CpG was coated onto the positively charged IR-7-lipo via electrostatic interactions. After HA-CpG absorption, the average hydrodynamic diameter increased to 129.7 ± 3.6 nm (Figure 2A). The obtained IR-7-lipo/HA-CpG nanoparticles dispersed as a well-defined spherical shape and homogeneous distribution by TEM image.

As expected, the IR-7-lipo/HA-CpG nanoparticles were negatively charged (-25.0 mV) (Figure 2B). The charge reversal after addition of HA-CpG further confirmed that HA-CpG was successfully coated onto IR-7-lipo.

Next, to verify the photothermal conversion capability of IR-7-lipo, temperature trends of IR-7-lipo upon NIR laser (808 nm, 2.0 W cm⁻²) irradiation were tested. As displayed in Figure 2C, IR-7 showed strong photothermal conversion efficiency (20.6% ± 1.2%) under 808 nm laser exposure, indicating encapsulation in liposomes did not influence the photothermal effect of IR-7. The photothermal conversion efficiency, η , was calculated using the following equation:

$$\eta = \frac{hA\Delta T_{\max} - Q_s}{I(1 - 10^{-A_\lambda})}$$

where h is the heat transfer coefficient, A is the surface area of the container, ΔT_{\max} is the temperature change between the equilibrium temperature and the ambient temperature, Q_s expresses heat dissipated from light absorbed by the quartz sample cell itself, which is measured using a quartz cuvette cell containing pure water without IR-7-lipo, I is the laser power, and A_λ is the absorbance of IR-7-lipo (25 μ g mL⁻¹) at the wavelength of 808 nm.

The temperature increased rapidly within a short time and then reached a plateau (Figure 2D). The temperature rising rate and plateau largely depended on the concentration of IR-7. When the concentration of IR-7 in IR-7-lipo was 25 μ g mL⁻¹, the temperature could increase to approximate 50 °C, whereas the temperature of 5% glucose was almost unchanged. These results suggested that IR-7-lipo could induce significant hyperthermia and lead to irreversible damages of cancer cells. These findings verified the great potential for effective PTT of IR-7-lipo.

Considering the strong NIR absorbance and *in vitro* PTT effect of IR-7-lipo, we next investigated its capability of *in vitro* photothermal ablation of cancer cells under NIR laser exposure. The PTT activity of IR-7-lipo was evaluated in murine colon cancer cell line CT26. The cells were incubated with IR-7-lipo and then irradiated with 808 nm laser for 5 min at the power density of 1.0 W cm⁻². CT26 Cells incubated with IR-7-lipo without NIR irradiation and cells incubated with 5% glucose with NIR irradiation were performed as controls. Subsequently, the cells were stained with calcein-AM and propidium iodide (PI) to identify living and dead cells. As shown in Figure 3A, of the strong green fluorescence signal was observed in cells incubated with 5% glucose with or without NIR irradiation and also in cells incubated with

IR-7-lipo without NIR irradiation, suggesting both IR-7-lipo and laser irradiation alone were non-toxic to cells. In marked contrast, upon 808 nm laser irradiation, IR-7-lipo-treated cells only exhibited strong red fluorescence signal. This indicated that IR-7-lipo could induce significant photothermal cytotoxicity in cancer cells upon NIR irradiation, killing almost all cancer cells. These results were further validated by FCM analysis (Figure 3A). Furthermore, IR-7-lipo induced significant necrosis (~73.05%) to CT26 cells upon laser irradiation (Figure S3, Supporting Information) while the other group induced none or little necrosis (< 8%) (Figure 3C). These results demonstrated that IR-7-lipo could effectively damage cancer cells through hyperthermia and could be applied as an effective and safe PTT agent.

Apoptosis, an intrinsic mechanism for programmed cell death, is regulated by a variety of cellular signaling pathways. During apoptotic death, cells are neatly carved up by caspases, packaged into apoptotic bodies, and then removed by phagocytosis [20]. This event is associated with the release of potent anti-inflammatory cytokines like transforming growth factor- β (TGF- β), prostaglandin E2 (PGE2), or platelet-activating factors as a mechanism to avoid immune activation [22-25]. Therefore, apoptosis is unanimously considered as an immunologically silent type of cell death. In contrast to apoptosis, necrosis has long been described as a consequence of extreme physicochemical stress, such as heat, osmotic shock, mechanical stress, and freeze-thawing, and was therefore classified as uncontrolled or accidental cell death. Necrosis is morphologically characterized by vacuolation of the cytoplasm, swelling of organelles, plasma membrane rupture and subsequent cellular collapse [26-28]. These processes can lead to the antigen release which may serve as the immunogen for the vaccine. The loss of membrane integrity and release of intracellular content including DAMPs (HMGB1, IL-1a, uric acid, DNA fragments, mitochondrial content, and ATP) grant necrotic cells the ability to induce an inflammatory response [29]. Some reports have demonstrated that this inflammatory response in the extracellular space may sometimes prevent nearby phagocytes from locating and eliminating the dead cells by phagocytosis, thus inducing local immunosuppression in the necrotic tissues [30]. Therefore, an alternative inflammatory response maybe needed to be constructed in the surrounding tissue to attract APCs to the necrotic tissues for initiating the immune response.

In this study, we combined HA-CpG, a multivalent immunoadjuvant with PTT to potentiate immune response against cancer. First, HA-CpG

could create an alternative inflammatory environment similar to bacterial infections to attract APCs. And second, HA-CpG could simultaneously act as an immunoadjuvant could be recognized by APCs, and promote APCs activation/maturation to amplify the subsequent immune responses. IR-7-lipo-based PTT induced necrosis of cancer cells and provided

tumor-associated antigens for APCs to trigger anti-tumor immune responses. Furthermore, DAMPs released from necrotic cancer cells after PTT could also stimulate PRRs, promote APCs activation/maturation and assist in the subsequent antigen processing and presentation.

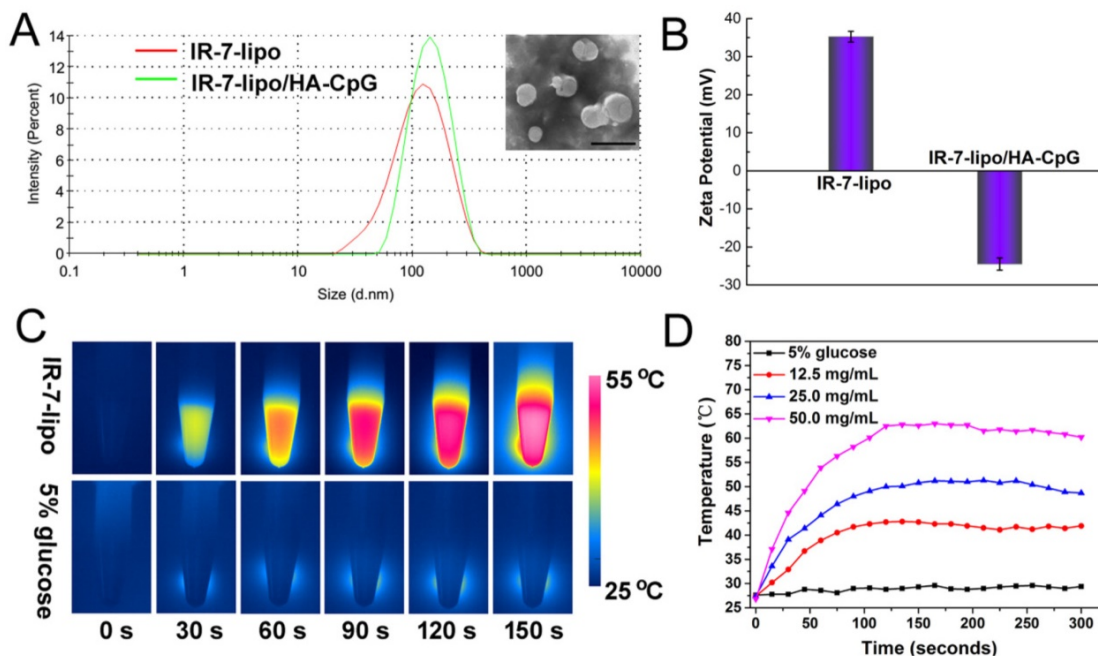


Figure 2. Preparation and characterization of IR-7-lipo and IR-7-lipo/HA-CpG. (A) Hydrodynamic size distributions of IR-7-lipo and IR-7-lipo/HA-CpG by DLS measurements. Inset: TEM image of IR-7-lipo/HA-CpG, scale bar = 200 nm. (B) Zeta potential of IR-7-lipo and IR-7-lipo/HA-CpG. Error bars represent variations among three independent measurements. (C) IR thermal images of IR-7-lipo (25 $\mu\text{g mL}^{-1}$ of IR-7) and 5% glucose upon 808 nm laser irradiation (2.0 W cm^{-2}) monitored by an IR thermal camera. (D) Real-time temperature profiles of IR-7-lipo at various concentration irradiated with 808 nm laser (2.0 W cm^{-2}).

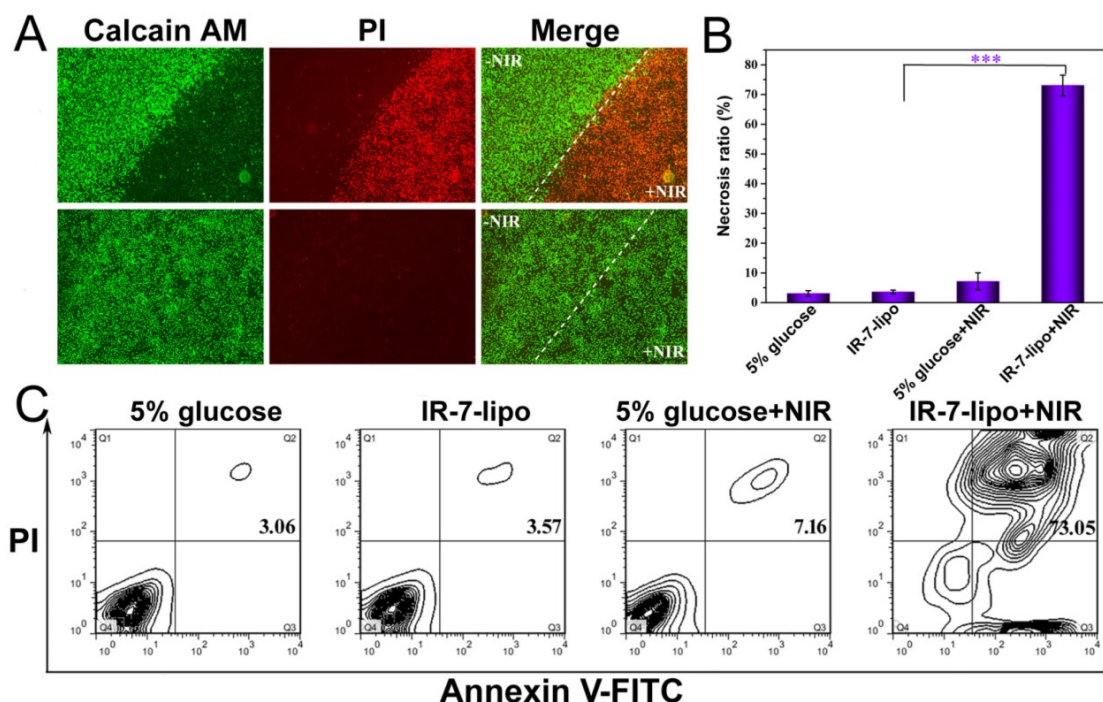


Figure 3. *In vitro* photothermal cytotoxicity in CT26 cells. (A) Fluorescence images of CT26 cells. LIVE/DEAD assay was performed after various treatments. The viable cells could be stained with Calcein AM (green), whereas the dead cells were labeled with PI (red). Scale bar = 200 μm . (B, C) FCM analysis of CT26 cells after different treatments. Positive FITC-Annexin V and PI cells were defined as late apoptosis/necrosis. $***p < 0.001$.

Next, we focused on evaluating immunostimulatory activities of the combination IR-7-lipo with HA-CpG (IR-7-lipo/HA-CpG nanoparticles). As professional APCs, DCs play a pivotal role in the initiation of innate and adaptive immunities. The expression of co-stimulatory molecules (CD40, CD80, CD83, CD86), the hallmark of DCs maturation, is critical for the migration of DC and subsequent antigen presentation [31]. Therefore, we first studied the effects of IR-7-lipo/HA-CpG on DC maturation *in vitro*. BMDCs were isolated from mice and incubated with IR-7-lipo/HA-CpG for 24 h. The maturation effect was assessed by analyzing the expression of the co-stimulatory molecules using Flow cytometry. As shown in Figure 4A and B (also Figure S4, Supporting Information), the expression of the co-stimulatory molecules CD40 and CD86 was significantly up-regulated on the BMDCs treated with IR-7-lipo/HA-CpG after laser exposure, validating that the pathogen-mimicking substances can enhance the activation and the maturation of APCs.

Following the recognition and ingestion of the tumor-associated antigen peptides by the APCs, these peptides needed to be presented to T cells via major histocompatibility complex (MHC) molecules, which are cell surface glycoproteins that play a fundamental

role in the regulation of innate and adaptive immune responses. There are two primary classes of MHC molecules. MHC class I molecules are necessary for the presentation of peptide antigens generated mainly from degradation of cytosolic proteins by the proteasome to CD8+ T cells [32-33]. MHC class II are a family of molecules normally found on APCs such as DCs, mononuclear phagocytes, some endothelial cells, and B cells. Their function is to bind peptides digested in lysosomes and display these antigen peptide fragments to CD4+ T cells [34]. Thus, we further evaluated the expression of MHC molecules on the surface of BMDCs after culturing with CT26 cells, which were pre-incubated with different formulations. As shown in Figure 4C and D, BMDCs incubation with the necrotic CT26 cells induced by IR-7-lipo/HA-CpG treatment and laser irradiation had a significant increase in the expression of both MHC class I and MHC class II molecules. This suggested that combination of PTT with HA-CpG could contribute to antigen peptides presentation. We also evaluated multiple cytokines including TNF- α , IL-12 and IL-6 in the serum after various treatments. As shown in Figure 5, the secretion levels of all three cytokines exhibited apparent elevation after IR-7-lipo/HA-CpG+NIR treatment.

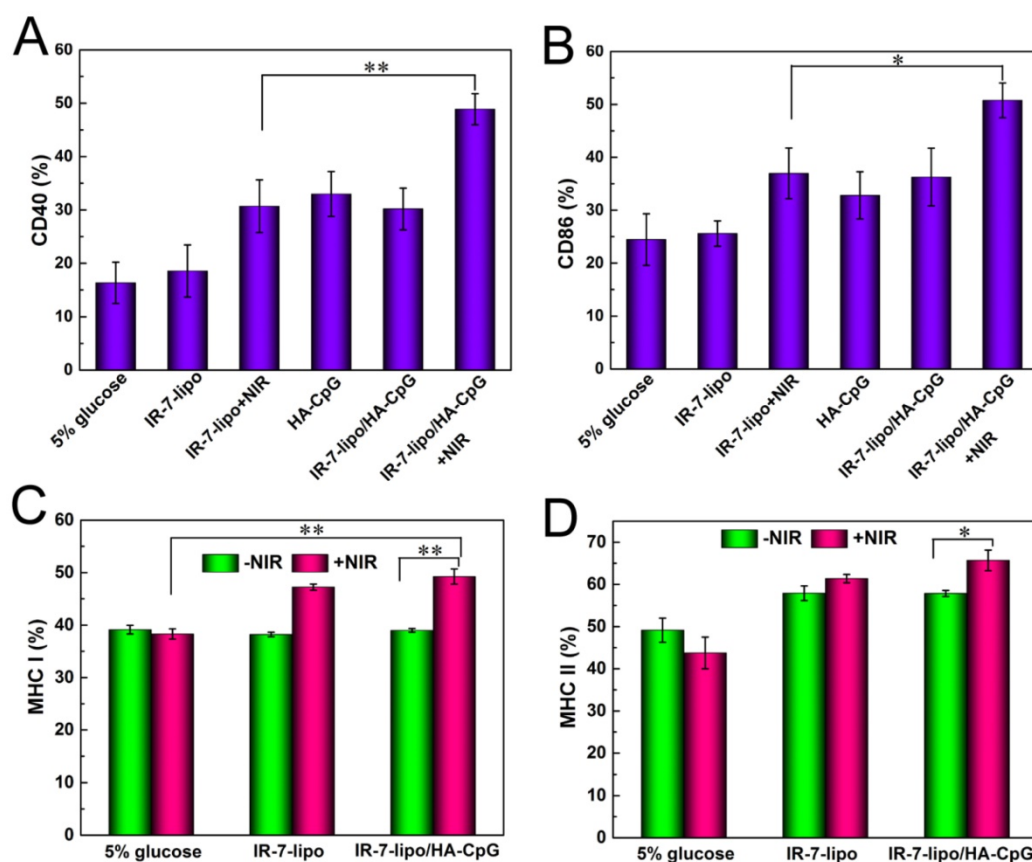


Figure 4. BMDCs maturation and antigen presentation assay. (A, B) Quantification of expression levels of CD40 and CD86 on the surface of BMDCs after various treatments. (C, D) Quantification of expression levels of MHC I and MHC II on the surface of BMDCs after different treatments. * $p < 0.05$, ** $p < 0.01$.

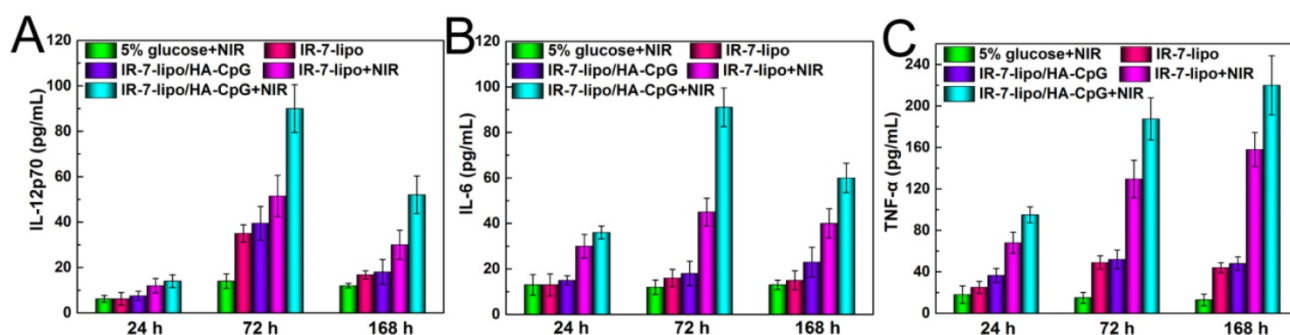


Figure 5. Cytokine levels of IL-12 (A), IL-6 (B), TNF- α (C) in sera from mice isolated at 24, 72 and 168 h post different treatments. Three mice were measured in each group.

It is well-known that tumor cells are located in an immunosuppressive micro-environment, containing large numbers of infiltrating immunosuppressive cells (Treg cells, MDSC and M2 macrophages) and cytokines (IL-10, TGF- β) hindering effective antitumor immune responses. Therefore, we performed further analysis of the immune response by examining the profiles of tumor-infiltrating leukocytes in tumors after various treatments. First, BALB/c mice were subcutaneously inoculated with CT26 murine colon cancer cells in their right flanks. When the tumor reached ~ 100 mm³, these tumors were injected with different formulations, and some of them were irradiated with an 808 nm laser at 2 W cm⁻² for 5 min. The mice were sacrificed 48 h after injection, the tumors were excised, and the immune cell populations within the tumor microenvironment were evaluated by Flow cytometry.

It was previously demonstrated that the necrosis induced by PTT could evoke acute inflammation. Therefore, we first evaluated the population of leukocytes responsible for the innate immune response (DCs and macrophages) in tumors after various treatment. As shown in Figure 6A (also Figure S5, Supporting Information), IR-7-lipo plus laser exposure led to a significant increase in the percentage of tumor-infiltrating DCs. The percentage of CD11b+CD11c+ macrophages in the tumors after IR-7-lipo/HA-CpG plus laser exposure treatment was nearly 1.6-fold of that in the 5% glucose under laser treatment. Notably, we also observed PTT plus HA-CpG (IR-7-lipo/HA-CpG) upon laser irradiation was much more effective in increasing the percentage of macrophages than IR-7-lipo plus laser exposure treatment (Data not shown). These results implied that the double-inflammation response induced by PTT and HA-CpG was much more effective in attracting DCs and macrophages to tumor areas than PTT alone.

MDSCs (CD11b+Gr1+), a heterogeneous population of immature myeloid cells, are an important class of immunosuppressive cells. MDSCs

accumulate during inflammation and in tumors and exert inhibitory function on immune responses. MDSCs regulate immune responses by several distinct mechanisms, such as modulating cytokine production by macrophages, depleting arginine, upregulating the production of immune-suppressive factors, overexpressing anti-inflammatory cytokines (TGF- β and IL-10), inducing apoptosis of CD8+ T cells, suppressing proliferation and cytokine production by T cells and natural killer cells, as well as inducing other immunosuppressive cells (Treg cells and M2 macrophages) [35-38]. We therefore profiled the tumor-infiltrating MDSCs after various treatments. As displayed in Figure 6B, upon laser exposure, the percentage of MDSCs increased significantly in tumors treated with IR-7-lipo. The percentage of MDSCs after PTT treatment alone was much higher than that of all other groups and was about 3-fold compared to that in 5% glucose plus laser exposure. These results implied that PTT alone could significantly exacerbate the immunosuppression of tumor micro-environment, which was consistent with our previous hypothesis that necrosis may induce local immunosuppression. Interestingly, after combined PTT with immunoadjuvant HA-CpG, the number of MDSCs was largely decreased and was 2.0-fold less compared to that of IR-7-lipo PTT treatment alone. After combination therapy, the percentage of MDSCs remarkably decreased, indicating that an alternative inflammatory response was necessary to promote immune responses after PTT treatment.

In addition to MDSC, CD4+ CD25+ Foxp3+ regulatory T (Treg) cells in the tumor micro-environment can also hamper effective anti-tumor immune responses. Therefore, we also investigated the percentage change of Treg cells after various treatments. Following intra-tumoral administration of IR-7-lipo or IR-7-lipo/HA-CpG, the percentage of Treg cells in the tumor increased considerably (Figure 6C). However, after 808 nm laser exposure, IR-7-lipo+NIR treatment induced about

7-fold more Treg cells compared to that in 5% glucose plus laser exposure, indicating PTT alone may promote immunosuppression in tumors. Interestingly, after PTT combined with HA-CpG, the percentage of Treg cells in the tumor remarkably decreased and almost returned to the normal condition. These results implied the pro-inflammatory immunoadjuvants might reverse the immunosuppressive tumor micro-environment induced by PTT alone.

Among all the lymphocytes, the activated CD8+CD69+ T cells (Cytotoxic T Lymphocytes, CTL)

are considered critical effector cells in tumor inhibition following immunotherapy. CD8+CD69+ T cells can release cytotoxins perforin, granzymes, and granulysin, which eventually lead to apoptosis of cancer cells [11, 39]. In the subsequent experiments, we further determined the number of tumor-infiltrating CD8+CD69+ T cells post treatment. IR-7-lipo/HA-CpG plus laser irradiation treatment significantly increased the percentage of infiltrating CD8+ T cells compared to other treatments (Figure 6D).

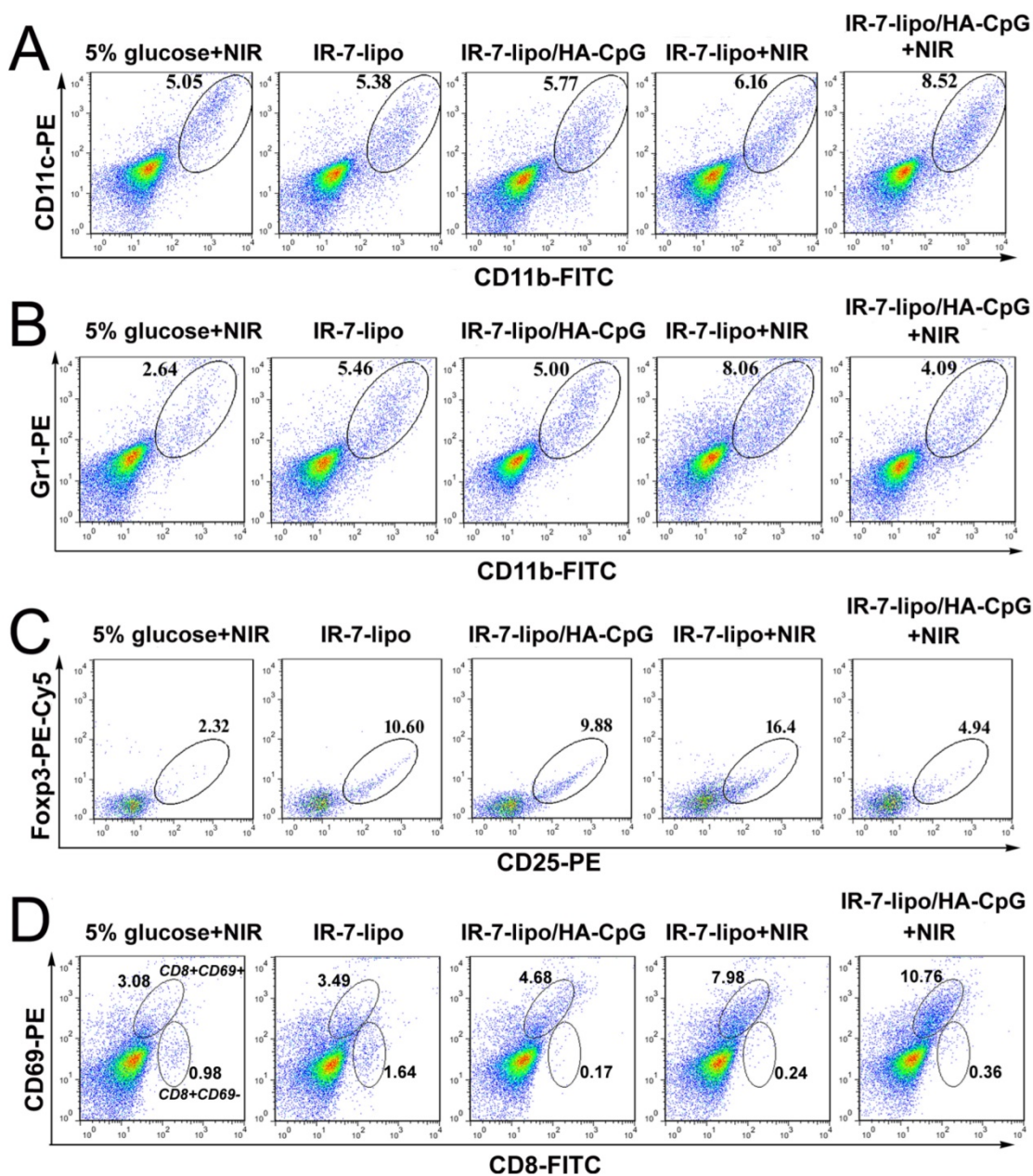


Figure 6. Regulation of tumor micro-environment. The tumor-infiltrating leukocyte profiles in tumors were analyzed by FCM plots of (A) DCs (CD11b+CD11c+). (B) MDSCs (CD11b+Gr1+). (C) CD4+ Treg cells (CD4+CD25+Foxp3+). (D) Activated CD8+ T cells (CD8+CD69+). *p < 0.05, **p < 0.01. The experiments were performed in triplicate with three different mice in each group.

Next, we examined whether IR-7-lipo/HA-CpG-mediated photothermal immunotherapy could exert systemic immune responses. The activated CD4+CD69+ T cells and CD8+CD69+ T effector cells in spleen were investigated by FCM after various treatments. As displayed in Figure 7 (also Figure S6, Supporting Information), IR-7-lipo/HA-CpG treatment upon laser exposure, significantly increased the percentages of both CD4+ T cells and CD8+ T effector cells in spleen, showing that the combination of PTT and immunotherapy could stimulate systemic anti-tumor immune response.

Collectively, these results indicated that PTT ablation and immunoadjuvant HA-CpG had combined effects on the activation of CD8+ T effector cells and relieved the immunosuppressive micro-environment of tumor. The combination of PTT and immunotherapy displayed more effective systemic immunity against tumors compared to PTT, which alone created a much stronger immunosuppressive tumor micro-environment.

Encouraged by the excellent PTT effect and high immune activity of IR-7-lipo/HA-CpG, we further examined the *in vivo* anti-tumor therapeutic effect of IR-7-lipo/HA-CpG. After the tumor sizes reached approximate 100 mm³, 5% glucose, IR-7-lipo, or IR-7-lipo/HA-CpG were administered by a single intratumoral injection. The tumors were then irradiated by the 808 nm laser at a power density of 2 W cm⁻² for 5 min. The temperature changes of tumors were monitored real-time by an IR thermal camera

during laser irradiation. As presented in Figure 8A and B, upon 808 nm laser exposure, mice treated with IR-7-lipo or IR-7-lipo/HA-CpG showed localized heating in the tumor region, and the temperature on the tumor areas rapidly increased to 50 °C that was high enough to ablate tumors *in vivo*. In comparison, the tumor temperatures of mice injected with 5% glucose exhibited little rise during 5 min of laser irradiation (below 40°C), indicating that 808 nm laser by itself could not induce sufficient heating. In the next 15 days, the tumor sizes and mouse body weights were recorded every 3 days. The tumors treated with IR-7-lipo/HA-CpG plus 808 nm laser irradiation shrank and became black scars at day 2. The representative photos of mice after different treatments are displayed in Figure S7 (Supporting Information). It is evident from Figure 8C and D, that the tumors treated with 5% glucose upon laser irradiation, IR-7-lipo and IR-7-lipo/HA-CpG without NIR laser exposure grew rapidly. The mice receiving IR-7-lipo plus 808 nm laser treatment or IR-7-lipo/HA-CpG plus 808 nm laser treatment exhibited significant delayed tumor growth, indicating IR-7-lipo-mediated PTT could effectively relieve the tumor growth. Notably, tumor growth after IR-7-lipo/HA-CpG plus laser treatment was much slower than that in mice treated with IR-7-lipo plus NIR laser, further confirming that the combination of PTT and immunotherapy provided a significant benefit to cancer treatment.

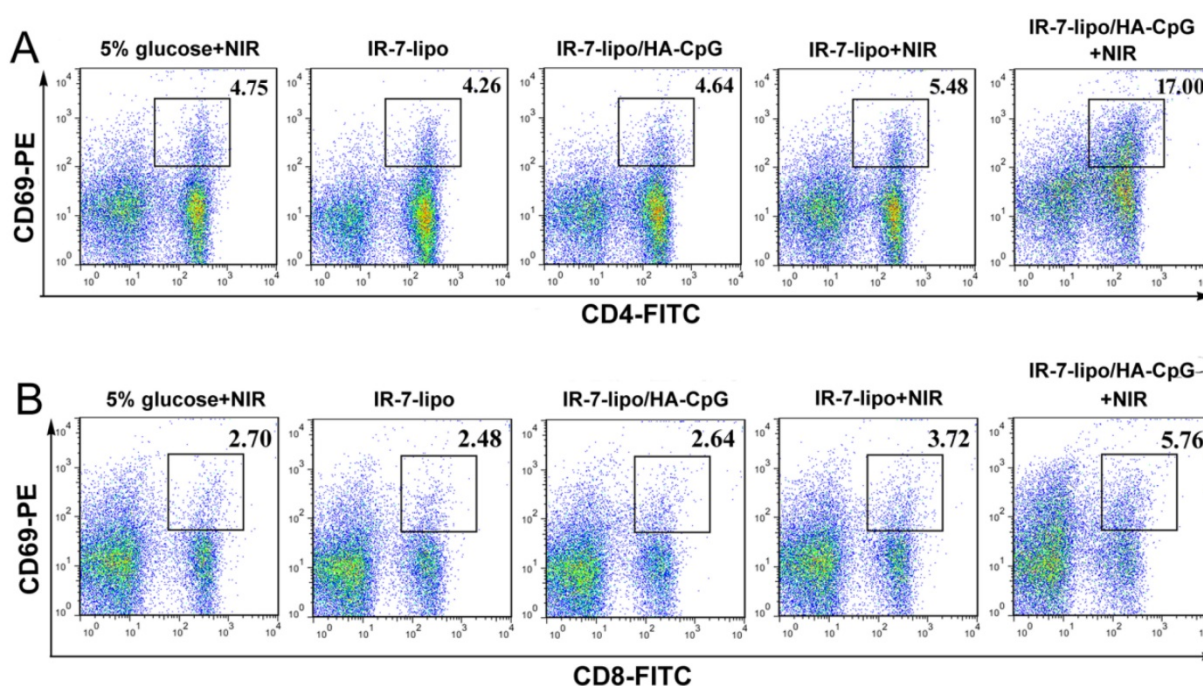


Figure 7. Antitumor systemic immunity. FCM plots of (A) activated CD4+ T cells (CD4+CD69+). (B) Activated CD8+ T cells (CD8+CD69+). **p* < 0.05, ***p* < 0.01. The experiments were performed in triplicate with three different mice in each group.

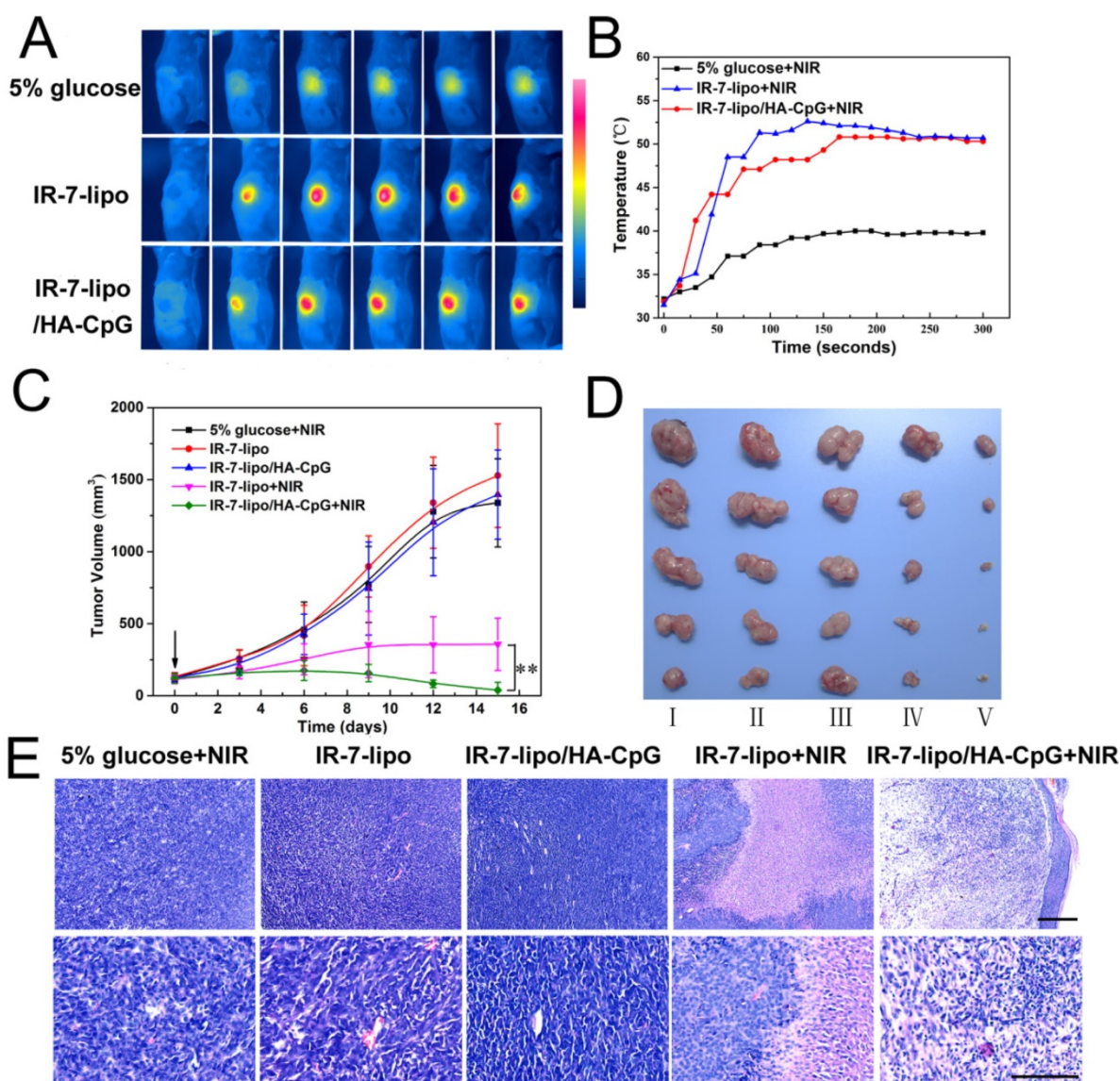


Figure 8. *In vivo* combination of photothermal and immunotherapy in CT26 colon cancer model. (A) IR thermal images of CT26 tumor-bearing mice under 808 nm laser irradiation (2.0 W cm^{-2}) taken at different time intervals. (B) Temperature increase profiles of tumor tissues in mice monitored by the IR thermal camera during laser irradiation (808 nm , 2.0 W cm^{-2}). (C) Tumor growth curves after various treatments. $**p < 0.01$. (D) Images of tumors after treatment with different formulations at day 15. I, 5% glucose + NIR; II, IR-7-lipo; III, IR-7-lipo/HA-CpG; IV, IR-7-lipo + NIR; V, IR-7-lipo/HA-CpG + NIR. (E) H&E staining of tumor tissues after various treatments. The scale bar indicated $100 \mu\text{m}$.

We also evaluated the anti-tumor efficacies of various treatments by hematoxylin and eosin (H&E) staining. Figure 8E demonstrates that neither obvious damage nor inflammation occurred in mice from 5% glucose with laser exposure, IR-7-lipo and IR-7-lipo/HA-CpG without laser treatment. In marked contrast, necrosis was observed in the center of the tumors after IR-7-lipo plus 808 nm laser treatment, while the surrounding tumor cells kept growing. Interestingly, nearly no tumor nidus was found in the mice after treatment with IR-7-lipo/HA-CpG plus laser irradiation.

During the period of treatments, the body weights of mice, which partially reflected the treatments-induced toxicity, were monitored. The

body weights after different treatments were not significantly different, suggesting that PTT treatment with IR-7-lipo was reasonably well-tolerated. Additionally, major organs including heart, liver, spleen, lung, and kidney of each group were collected after treatments for histology analysis (Figure S8, Supporting Information). No noticeable toxic effects were observed from H&E staining, implying the high biocompatibility of the combination therapy of PTT and immunotherapy.

Inspired by the therapeutic outcome of the combination therapy of PTT and immunotherapy, we investigated whether these effects would be beneficial to prevent tumor metastasis. We inoculated the first tumor on the right flank of each mouse. Ten days

later, when the first tumor reached $\sim 200 \text{ mm}^3$ (mimic the large bulk tumor), a second tumor was inoculated on the left flank. After 2 days, the first tumor was treated with IR-7-lipo+NIR, IR-7-lipo/HA-CpG+NIR or removed by surgery. The growth of the secondary tumor was monitored. As shown in Figure S9, after surgery treatment, the original tumor site in the right flank showed tumor recurrence and the second tumor inoculated in the left flank exhibited continuous growth. After IR-7-lipo+NIR or IR-7-lipo/HA-CpG+NIR treatment, no tumor growth was observed in the left flank. Notably, after IR-7-lipo/HA-CpG+NIR treatment, the original tumor in the right flank shrank and vanished. Due to the large bulk of the tumor, the surviving tumor cells after IR-7-lipo+NIR treatment continued to grow rapidly.

Conclusions

We demonstrated an endogenous vaccination strategy based on fluorophores IR-7 and multivalent immunoadjuvants HA-CpG, which effectively regulated tumor micro-environment for synergistic PTT and immunotherapy of cancer. Under laser irradiation, the IR-7-lipo/HA-CpG triggered remarkable tumor cell death *in vitro*. The *in vivo* experiments also revealed improved tumor inhibition with minimal systemic toxicity. Taken together, our results showed that the combinational PTT and immunotherapy strategy exhibits a synergistic anti-tumor effect with excellent biocompatibility. Our work also suggested that, compared with surgical resection, integration of PTT and immunotherapy is advantageous for triggering the adaptive immune responses against tumor residues.

Abbreviations

NIR: near-infrared; PTT: photothermal therapy; IR-7-lipo: fluorophore-loaded liposomes; BMDC: bone marrow-derived dendritic cells; FCM: flow cytometry; CNTs: carbon nanotubes; ICG: Indocyanine Green; DAMPs: danger-associated molecular patterns; PRRs: pattern-recognition receptors; Treg: regulatory T cells; MDSCs: myeloid derived suppressor cells; TGF- β : transforming growth factor- β ; ODNs: oligodeoxynucleotides; CpG: cytosine-phosphate-guanine; TLR9: Toll-like receptor 9; APCs: antigen presenting cells; HA-CpG: CpG ODNs grafted hyaluronic acid; DSPC: 1,2-distearoyl-sn-glycero-3-phosphocholine; DOTAP: 1,2-dioleoyl-3-trimethylammonium-propane; NHS: N-hydroxysuccinimide; EDCI: 1-(3-dimethylaminopropyl)-3-ethylcarbodiimide hydrochloride; HA: Sodium hyaluronate; FBS: fetal bovine serum; MES: 2-(N-morpholino) ethanesulfonic acid; DLS: dynamic light scattering; TEM: transmission electron

microscopy; GM-CSF: granulocyte macrophage colony-stimulating factor; TNF- α : Tumor necrosis factor- α ; SD: standard deviation; PGE2: prostaglandin E2; MHC: major histocompatibility complex; CTL: Cytotoxic T Lymphocytes; H&E: hematoxylin and eosin.

Supplementary Material

Supplementary figures.

<http://www.thno.org/v08p0860s1.pdf>

Acknowledgments

This work was financially supported by National Program for Support of Top-notch Young Professionals and Distinguished Young Scholars of Sichuan University (2015SCU04A42).

Competing Interests

The authors have declared that no competing interest exists.

References

- Cheng L, Wang C, Feng L, Yang K, Liu Z. Functional Nanomaterials for Phototherapies of Cancer. *Chem Rev.* 2014;114: 10869-939.
- Liang C, Diao S, Wang C, Gong H, Liu T, Hong G, et al. Tumor Metastasis Inhibition by Imaging-guided Photothermal Therapy with Single-Walled Carbon Nanotubes. *Adv Mater.* 2014; 26: 5646-52.
- Deng H, Dai F, Ma G, Zhang X. Theranostic Gold Nanomicelles Made from Biocompatible Comb-Like Polymers for Thermochemotherapy and Multifunctional Imaging with Rapid Clearance. *Adv Mater.* 2015; 27:3645-53.
- Sheng Z, Hu D, Zheng M, Zhao P, Liu H, Gao D, et al. Smart Human Serum Albumin-Indocyanine Green Nanoparticles Generated by Programmed Assembly for Dual-Modal Imaging-Guided Cancer Synergistic Phototherapy. *ACS Nano.* 2014; 8:12310-22.
- Huang P, Gao Y, Lin J, Hu H, Liao H. S, Yan X, et al. Tumor-Specific Formation of Enzyme-Instructioned Supramolecular Self-Assemblies as Cancer Theranostics. *ACS Nano.* 2015; 9: 9517-27.
- Guo L, Yan D-D, Yang D, Li Y, Wang X, Zalewski O, et al. Combinatorial Photothermal and Immuno Cancer Therapy Using Chitosan-Coated Hollow Copper Sulfide Nanoparticles. *ACS Nano.* 2014; 8: 5670-81.
- Krysko DV, Agostinis P, Krysko O, Garg AD, Bachert C, Lambrecht BN, et al. Emerging Role of Damage-Associated Molecular Patterns Derived from Mitochondria in Inflammation. *Trends Immunol.* 2011;32: 157-64.
- Garg AD, Nowis D, Golab J, Vandenabeele P, Krysko DV, Agostinis P. Immunogenic Cell Death Damps and Anticancer Therapeutics: an Emerging Amalgamation. *BBA-Rev Cancer.* 2010;1: 53-71.
- Chen G. Y, Nuñez G. Sterile Inflammation: Sensing and Reacting to Damage. *Nat Rev Immunol.* 2010; 10: 826-37.
- Butt AQ, Mills KHG. Immunosuppressive Networks and Checkpoints Controlling Antitumor Immunity and Their Blockade in the Development of Cancer Immunotherapeutics and Vaccines. *Oncogene.* 2014;33: 4623-31.
- Wang C, Xu L, Liang C, Xiang J, Peng R, Liu Z. Immunological Responses Triggered by Photothermal Therapy with Carbon Nanotubes in Combination with Anti-CTLA-4 Therapy to Inhibit Cancer Metastasis. *Adv Mater.* 2014; 26: 8154-62.
- Kawai T, Akira S. The Role of Pattern-Recognition Receptors in Innate Immunity: Update on Toll-Like Receptors. *Nat. Immunol.* 2010; 11: 373-84.
- Kumagai Y, Takeuchi O, Akira S. TLR9 as a Key Receptor for the Recognition of DNA. *Adv Drug Delivery Rev.* 2008; 60: 795-804.
- Shirota Y, Shirota H, Klinman DM. Intratumoral Injection of CpG Oligonucleotides Induces the Differentiation and Reduces the Immunosuppressive Activity of Myeloid-Derived Suppressor Cells. *J Immunol.* 2012; 188: 1592-9.
- Zoglmeier C, Bauer H, Nörenberg D, Wedekind G, Bittner P, Sandholzer N, et al. CpG Blocks Immunosuppression by Myeloid-Derived Suppressor Cells in Tumor-Bearing Mice. *Clin Cancer Res.* 2011; 17: 1765-75.
- Kim S-Y, Heo M-B, Hwang G-S, Jung Y, Choi D-Y, Park Y, et al. Multivalent Polymer Nanocomplex Targeting Endosomal Receptor of Immune Cells for Enhanced Antitumor and Systemic Memory Response. *AngewChem Int Edit.* 2015; 28: 8139-43.

17. Luo S, Tan X, Fang S, Wang Y, Liu T, Wang X, et al. Mitochondria-Targeted Small-Molecule Fluorophores for Dual Modal Cancer Phototherapy. *Adv Funct Mater.* 2016; 17: 2826-35.
18. Roper, D, Ahn, W, Hoepfner, M. Microscale Heat Transfer Transduced by Surface Plasmon Resonant Gold Nanoparticles. *J Phys Chem C.* 2007; 111: 3636-41.
19. Kim S-Y, Heo M-B, Hwang G-S, Jung Y, Choi D. Y, Park Y, Lim Y-T. Multivalent Polymer Nanocomplex Targeting Endosomal Receptor of Immune Cells for Enhanced Antitumor and Systemic Memory Response. *Angew Chem Int Edit.* 2015; 28: 8139-43.
20. Marrache S, Tundup S, Harn DA, Dhar S. Ex Vivo Programming of Dendritic Cells by Mitochondria-Targeted Nanoparticles to Produce Interferon-Gamma for Cancer Immunotherapy. *ACS Nano.* 2013; 7: 7392-402.
21. Edinger AL, Thompson CB. Death by Design: Apoptosis Necrosis and Autophagy. *Curr Opin Cell Bio.* 2004; 6: 663-9.
22. Chen WJ, Frank ME, Jin W, Wahl SM. TGF-Beta Released by Apoptotic T Cells Contributes to an Immunosuppressive Milieu. *Immunity.* 2001;14: 715-25.
23. Fadok VA, Bratton DL, Konowal A, Freed PW, Westcott JY, Henson PM. Macrophages That Have Ingested Apoptotic Cells In Vitro Inhibit Proinflammatory Cytokine Production Through Autocrine Paracrine Mechanisms Involving TGF-Beta PGE2 and PAF. *J Clin Invest.* 1998; 101: 890-8.
24. Savill J, Fadok V. Corpse Clearance Defines the Meaning of Cell Death. *Nature.* 2000;407: 784-8.
25. Voll RE, Herrmann M, Roth EA, Stach C, Kalden JR, Girkontaite I. Immunosuppressive Effects of Apoptotic Cells. *Nature.* 1997; 390: 350-1.
26. Krysko DV, Berghe TV, D'Herde K, Vandenabeele P. Apoptosis and Necrosis: Detection Discrimination and Phagocytosis. *Methods.* 2008; 44: 205-221.
27. Krysko DV, Berghe TV, Parthoens E, D'Herde K, Vandenabeele P. Methods for Distinguishing Apoptotic from Necrotic Cells and Measuring Their Clearance. *Method Enzymol.* 2008; 442: 307-41.
28. Berghe, TV, Vanlangenakker N, Parthoens E, Deckers W, Devos M, Festjens N, et al. Necroptosis Necrosis and Secondary Necrosis Converge on Similar Cellular Disintegration Features. *Cell Death Differ.* 2010; 17: 922-30.
29. Kaczmarek A, Vandenabeele P, Krysko DV. Necroptosis: the Release of Damage-Associated Molecular Patterns and Its Physiological Relevance. *Immunity.* 2013; 38: 209-23.
30. Vakkila J, Lotze M. T. Inflammation and Necrosis Promote Tumour Growth. *Nat Rev Immunol.* 2004; 4: 641-648.
31. Janeway CA, Bottomly K. Signals and Signs for Lymphocyte Responses. *Cell.* 1994; 76: 275-85.
32. Rock KL, Gramm C, Rothstein L, Clark K, Stein R, Dick L, Hwang D, Goldberg AL. Inhibitors of the Proteasome Block the Degradation of Most Cell Proteins and the Generation of Peptides Presented on MHC Class I Molecules. *Cell.* 1994;78: 761-71.
33. Kovacsics-Bankowski M, Rock KL. A Phagosome-to-Cytosol Pathway for Exogenous Antigens Presented on MHC Class I Molecules. *Science.* 1995; 267: 243-46.
34. Rammensee HG. Chemistry Of Peptides Associated with MHC Class I and Class II Molecules. *Curr Opin Immunol.* 1995; 7: 85-96.
35. Gabrilovich DI, Nagaraj S. Myeloid-Derived Suppressor Cells as Regulators of the Immune System. *Nat Rev Immunol.* 2009; 9: 162-74.
36. Sinha P, Clements VK, Fulton AM, Ostrand-Rosenberg S. Prostaglandin E2 Promotes Tumor Progression by Inducing Myeloid-Derived Suppressor Cells. *Cancer Res.* 2007;67: 4507-13.
37. Serafini P, Mgebhoff S, Noonan K, Borrello I. Myeloid-Derived Suppressor Cells Promote Cross-Tolerance in B-Cell Lymphoma by Expanding Regulatory T Cells. *Cancer Res.* 2008; 68: 5439-49.
38. Ostrand-Rosenberg S. Myeloid-Derived Suppressor Cells: More Mechanisms for Inhibiting Antitumor Immunity. *Cancer Immunol Immun.* 2010; 59: 1593-600.
39. Chen Q, Xu L, Liang C, Wang C, Peng R, Liu Z. Photothermal Therapy with Immune-Adjuvant Nanoparticles Together with Checkpoint Blockade for Effective Cancer Immunotherapy. *Nat Commun.* 2016; 7: 13193.